Chinese Chemical Letters 34 (2023) 107900

Contents lists available at ScienceDirect

Chinese Chemical Letters

journal homepage: www.elsevier.com/locate/cclet

Highly efficient solid-state luminescence of carbonized polymer dots without matrix

Rui Li, Junjun Liu, Chunlei Xia, Tanglue Feng, Zhicheng Zhu, Bai Yang*

State Key Laboratory of Supramolecular Structure and Materials, College of Chemistry, Jilin University, Changchun 130012, China

ARTICLE INFO

Article history:
Received 8 July 2022
Revised 10 October 2022
Accepted 11 October 2022
Available online 17 October 2022

Keywords:
Carbonized polymer dots
Solid-state fluorescence
Matrix-free
High performance
Enhanced photoluminescence quantum yield

ABSTRACT

Development of high-performance solid state luminescent carbon-based nanomaterials remains challenging. Here, strong blue-green fluorescent carbonized polymer dots (CPDs) from *o*-aminobenzenethiol and thiosalicylic acid (oABT-TSA-CPDs) with an absolute photoluminescence quantum yield (PLQY) of 76% in solid state without matrix were synthesized. Through adjusting the reaction temperature and time, the PL centers were proved to be carbon core state and surface state associated to carbonyl group which was the source of strong fluorescence emission in solid state. The mechanism of the unique phenomenon of enhanced emission from ethanol solution (PLQY = 7%) to powder (PLQY = 76%) was investigated by analyzing the chemical properties and structures of oABT-TSA-CPDs at different temperatures and oABT-TSA-CPDs/PVC composites, and was confirmed as fixation of PL centers.

As a new type of fluorescent material, carbon dots (CDs) have attracted much attention in recent years due to their low toxicity, simple preparation, low cost, and excellent optical properties [1], leading to wide applications in many fields such as biomedicine [2], catalysis [3], optoelectronic devices [4–6]. CDs always show strong photoluminescence (PL) in solution, but weak or no fluorescence in solid state, because of aggregation caused quenching (ACQ) effect resulting from fluorescence resonance energy transfer (FRET), interparticle coupled surface states, or direct $\pi-\pi$ interaction, which greatly limits their application in optoelectronic devices [7,8]. Consequently, it is highly desirable to achieve high-performance solid-state luminescent CDs.

Researchers usually dispersed CDs into matrix such as polymers [9–11], hydrotalcite [12,13], starch [14], mesoporous pipes [15] to avoid ACQ and realize composites of CDs with solid state luminescence. However, these methods need complicated procedures and low CDs doping. Carbonized polymer dots (CPDs) possess special core-shell nanostructures (carbon core and polymer-like shell), crosslinked polymer frames, which facilitate to increase the distance among the PL centers of CPDs and prevent ACQ [16].

In this work, we synthesized CPDs from *o*-aminobenzenethiol (oABT) and thiosalicylic acid (TSA). According to our previous work [17], the prepared CPDs were named as oABT-TSA-CPDs. The fluorescence centers of the oABT-TSA-CPDs came from carbon core state and surface state, which was the potential fluorescent chromophore associated with carbonyl group by analyzing micro-nanostructures of CPDs synthesized at different conditions. More importantly, the PLQY of oABT-TSA-CPDs powder (76%) was much higher than that of ethanol solution (7%) due to the fixation of PL centers and the crosslink enhanced emission (CEE) effect of hydrogen bonds in solid state, which was the biggest difference from other CDs like carbon quantum dots (CQDs), graphene quantum dots (GQDs) and some CPDs with high carbonization-degree.

Blue-green emissive oABT-TSA-CPDs with PLQY of 76% (Fig. S12c in Supporting information) in solid state without matrix were synthesized by one pot formic acid solvothermal treatment of oABT and TSA at 180 °C for 8 h, which showed blue emission in solution and strong blue-green fluorescence in powder (Fig. 1a). Transmission electron microscopy (TEM) images (Fig. 1b) showed oABT-TSA-CPDs were uniform quasi spherical nanoparticles with average diameter of 5.2 nm (Fig. S4a in Supporting information), and obvious lattice structures (inset image in Fig. 1b) with the spacing of 0.21 nm representing graphitic facet (101) [18]. oABT-TSA-CPDs powder behaved excitation-independent emission with peak at 477 nm and the shoulder peak at 499 nm (Fig. 1c). Besides, the ethanol solution of oABT-TSA-CPDs showed two obvious PL centers, one peak was at 407 nm under the excitation wavelength of 320-380 nm, the other peak was around 470 nm under 390-430 nm excitation (Fig. 1d). Additionally, the PL spectrum of oABT-TSA-CPDs in DMSO (Fig. S1 in Supporting information) also showed the two obvious emission centers. Most CDs showed weak or no emission in solid state but high fluorescence in solution [8]. However, the PLQY of oABT-TSA-CPDs solution was only 7%, which was much lower than that of

* Corresponding author.
E-mail address: byangchem@jlu.edu.cn (B. Yang).

https://doi.org/10.1016/j.cclet.2022.107900
1001-8417/

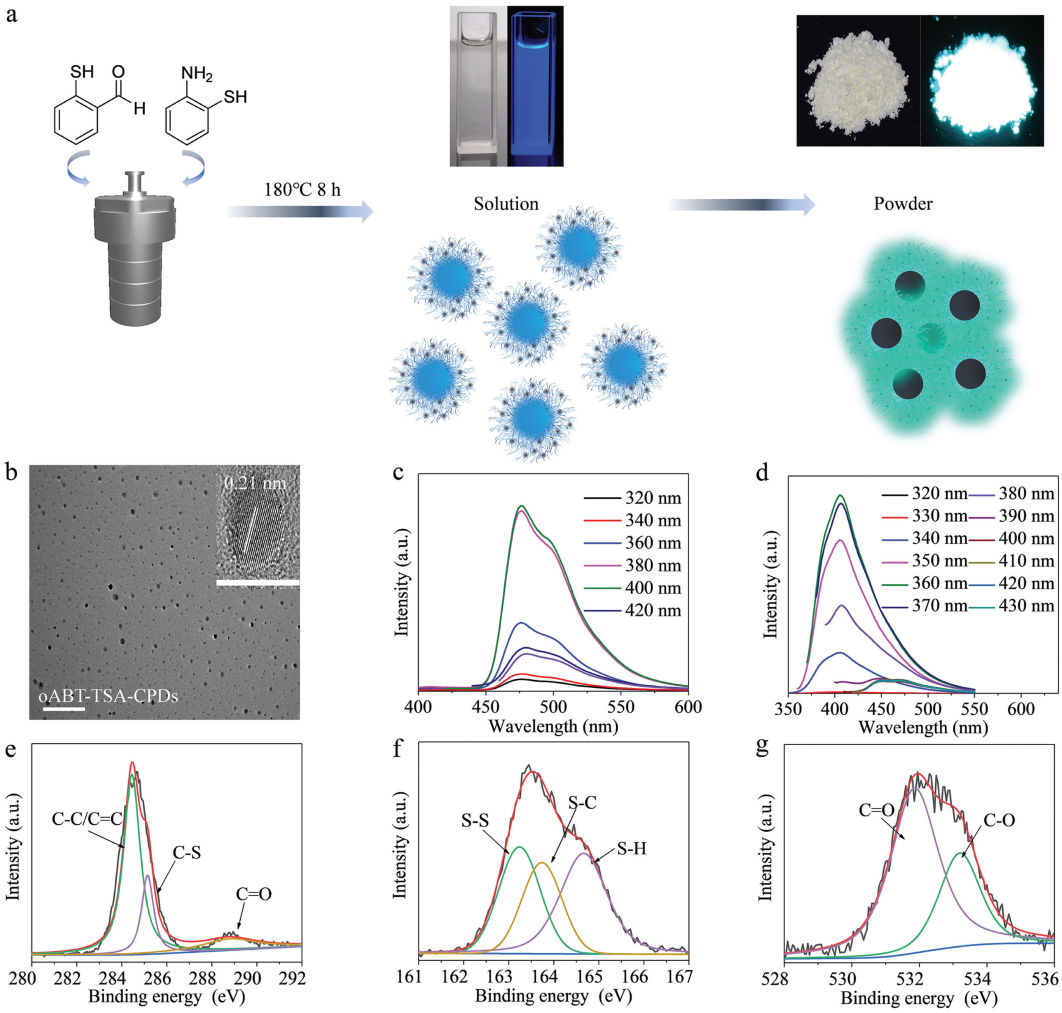

Fig. 1. (a) Synthesis and photos of oABT-TSA-CPDs in ethanol solution and powder (the fluorescent photographs captured under 365 nm UV light). (b) TEM image and HRTEM image (inset image) of oABT-TSA-CPDs (scale bar: 50 nm inset: 5 nm). (c) The PL spectra of oABT-TSA-CPDs powder under different excitation wavelength. (d) The PL spectra of oABT-TSA-CPDs ethanol oution under different excitation wavelength. (e-g) The high resolution XPS spectra of oABT-TSA-CPDs (C 1s, S 2p and O 1s, respectively).

the solid state (76%), and there were few related studies about this unique phenomenon. The PL mechanism would be explored in detail in this work.

The micro-nanostructures of oABT-TSA-CPDs were first investigated through elemental analysis, X-ray photoelectron spectroscopy (XPS) and Fourier transform infrared (FTIR) spectrum. The XPS spectrum indicated that oABT-TSA-CPDs mainly consisted of C, O, N and S (Fig. S2a in Supporting information), which was in agreement with the data of elemental analysis (Table S2 in Supporting information). The high-resolution C 1s spectrum (Fig. 1e) showed three types of C: C-C/C=C, C-S/C-O and C=O. S 2p spectrum (Fig. 1f) revealed three peaks: S-C, S-H and S-S. Additionally, O 1s appeared (Fig. 1g) two peaks of C-O and C=O and N 1s (Fig. S2b in Supporting information) showed two peaks of pyridinic N and graphitic N [19–23]. Consistent with the analysis of XPS data, FTIR spectrum (Fig. S3 in Supporting information) presented the stretching vibration of O-H at 3124 cm^{-1} with strong and broad absorption peak. And the peaks at 3015 cm^{-1}, 2550 cm^{-1}, 1680 cm^{-1}, 1410 cm^{-1}, 1260 cm^{-1}, 685 cm^{-1} and 491 cm^{-1} were attributed to the stretching vibration of =C-H, S-H, C=O, C-N, C-O-C, C-S and S-S, respectively [19–23]. According to the analysis of micro-nanostructures, we could conclude that after the assembling, polymerization, cross-linking, and carbonization under high temperature and high pressure, the oABT-TSA-CPDs formed and performing high PLQY in solid state.

Reaction temperature and reaction time could affect the assembling, polymerization, cross-linking and carbonization process of CPDs, which could affect the formation of PL centers [24]. Therefore, we first regulated reaction temperature to explore the concrete structures of PL centers for oABT-TSA-CPDs. CPDs-140 and CPDs-220 were prepared at 140 °C and 220 °C for 8 h while other reaction conditions remained constant. TEM images of CPDs-140, and CPDs-220 showed dot-shape with obvious lattice structure of 0.21 nm, indicating no distinct difference in core structure (Figs. 2a and b). The particle size of CPDs-140 was 5.1 nm, and CPDs-220 was slightly larger (6.1 nm) (Figs. S4b and c in Supporting information), which was associated with the high carbonization degree. With the low/high reaction temperature, the PL intensity of CPDs reduced, and the PLQY of CPDs-140 and CPDs-220 in solid state was only 8% and 3% (Figs. S12d and e in Supporting information), respectively. The photos of CPDs-140 and CPDs-220 (Fig. 2c) also showed weak emission. Generally, surface state was gradually formed with the reaction temperature increased, thus resulting in the increase of PLQY. However, the over-carbonization under high reaction temperature would destroy the surface state, and carbon core state would dominate the PL behavior of CPDs [24].

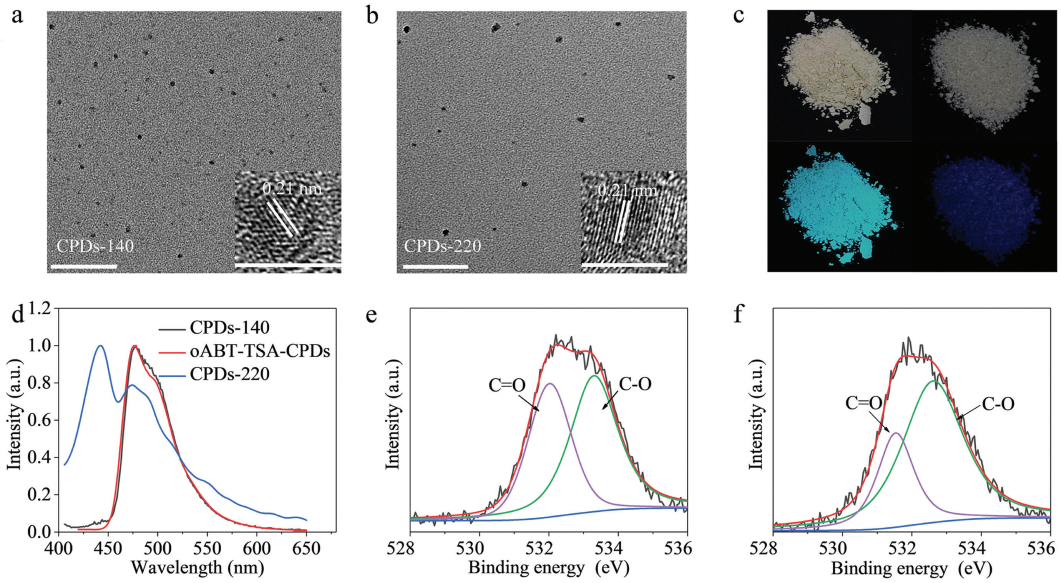

Fig. 2. (a, b) TEM images and HRTEM images (inset) of CPDs-140, CPDs-220, respectively (scale bar: 100 nm; inset 5 nm). (c) The photos of CPDs-140 (left) and CPDs-220 (right), taken under sunlight (upper panel) and UV light (lower panel). (d) PL spectra of CPDs-140, oABT-TSA-CPDs, CPDs-220 powder. (e, f) The high resolution O 1s XPS spectra of CPDs-140 and CPDs-220, respectively.

For CPDs-140 and oABT-TSA-CPDs, surface state was their main PL mechanism, while the PL of CPDs-220 was mainly governed by carbon core state. As shown in Fig. 2d, CPDs-140 and oABT-TSA-CPDs powder showed the same emission at 477 nm, but CPDs-220 powder showed fluorescent peak around 441 nm, which belong to carbon core state, and the shoulder peak at 476 nm was from surface state. Therefore, these CPDs possessed two PL centers, the fluorescent emission peak before 450 nm belong to carbon core state, while the emission peak after 450 nm belong to surface state. Generally, the PL of surface state tended to be solvent-dependent [25]. The PL spectrum of oABT-TSA-CPDs in DMSO solurion (Fig. S1) showed the peak at 470 nm was more affected by solvents, which further prove the surface state was the latter emission. However, the surface state in solution exhibited weak fluorescence, performing strong emission in solid state. More detailed explanation would be discussed in the following section.

Furthermore, XPS was used to study the concrete structures of fluorophore. The XPS spectrum (Figs. S2e and f in Supporting information) showed that CPDs-140 and CPDs-220 mainly consisted of C, O, N, and S. According to the analysis of the high-resolution C 1s, O 1s spectra of CPDs-140, oABT-TSA-CPDs, and CPDs-220, these CPDs had the same functional groups, but the amounts of these groups were different as shown in Table S3 (Supporting information). Consistent with the trend of PLQY, the relative contents of C=O (Figs. 2e and f) increased with increasing the reaction temperature and then decreased, which indicated C=O was the main fluorophore of oABT-TSA-CPDs, similar with the PL mechanism of most reported blue/green emissive CPDs [26].

On the other hand, we tuned reaction time to further confirm the concrete structures of PL centers for oABT-TSA-CPDs. CPDs-2H and CPDs-24H synthesized at 180 °C for 2 h and 24 h with the same raw materials, respectively. These two CPDs showed similar carbon core structure to oABT-TSA-CPDs (Figs. S5a and b in Supporting information), indicating the carbon core had been formed at the early reaction time or low reaction temperature due to the organic solvent which was conductive to dehydration and carbonization compared with water. However, CPDs-2H and CPDs-24H powder behaved weaker blue-green emission as shown in Fig. S5c (Supporting information). They showed emission peak at 477 nm (Fig. S5d in Supporting information), same with the PL spectrum of oABT-TSA-CPDs. But their PLQY were of 13% and 9% (Figs. S12a and b in Supporting information), respectively, much lower than that of oABT-TSA-CPDs. Because the short reaction time would result in the uncompleted formation of surface state, and the long reaction time could lead to excessive carbonization and destroy the surface state, which both caused weak PL emission. Consistent with the trend of PLQY, XPS data (Figs. S2c and d, Table S2 and Figs. S5e and f in Supporting information) also confirmed that the relative contents of C=O increased first and then decreased with the increase of reaction time.

Taken together, it was evident that oABT-TSA-CPDs had two PL centers, one was carbon core state with the fluorescent emission peak before 450 nm, the other was surface state with emission peak at 407 nm in solution and 477 nm in powder. Besides, the strong fluorescence of oABT-TSA-CPDs powder came from the surface state which was associated to fluorescent chromophore C=O.

From the above data, there were conspicuous differences of PL property between solution and solid-state. The emission of oABT-TSA-CPDs solution mainly showed carbon core state at 407 nm with low PLQY of 7% but performing strong surface state fluorescence at 477 nm with PLQY of 76% in solid-state, which was a unique phenomenon in CDs. It was obvious that the surface state played an important role in PL enhancement, thus the following investigation was mainly about the structures and properties of surface state.

The PLQY is relevant to the dissipation path of energy. Non-radiative dissipation causes low PLQY, showing weak emission, while radiatively recombination would conduct high PLQY [27,28]. To further investigate the PL mechanism of oABT-TSA-CPDs, the time-resolved PL decay curves of solution and powder were given (Fig. 3a). Generally, the non-radiative transition rate is much faster than radiative recombination and showed short lifetime. As shown in Fig. 3a, the solution showed a very short lifetime of 0.8 ns, while the powder could reach 3.47 ns, which indicated the energy mainly vanished through the non-radiative transition pathway in the solution, resulting in low PLQY. The radiative transition rate (K_r) and the non-radiative transition rate (K_{nr}) were calculated according to the lifetime and PLQY based on the followed formulas [29].

The results (Table S1) showed the powder exhibited larger K_r and smaller K_{nr}, indicating less non-radiative transition comparing

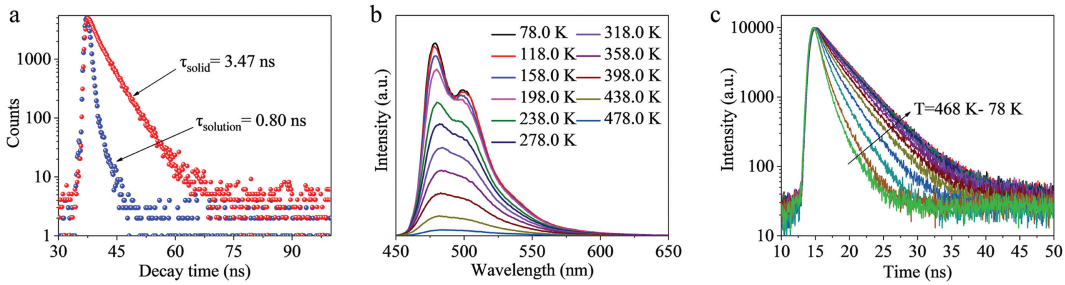

Fig. 3. (a) Time resolved PL decay curves of oABT-TSA-CPDs powder (red) and ethanol solution (blue). (b) PL spectra of oABT-TSA-CPDs powder at different temperature. (c) Time resolved PL decay curves of oABT-TSA-CPDs powder at different temperature.

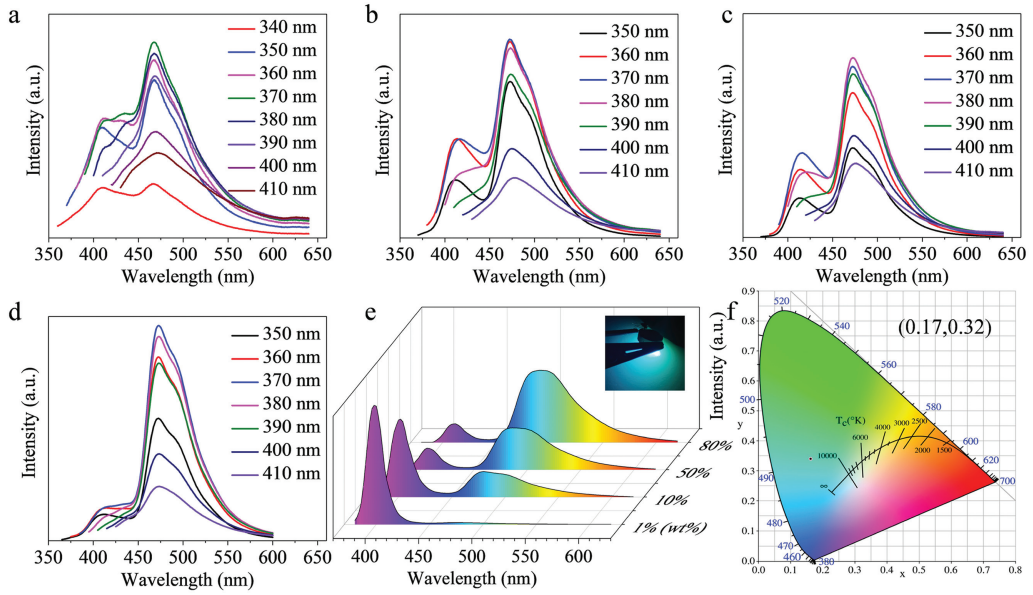

Fig. 4. (a-d) PL spectra of 1%, 3%, 5%, 10% (the mass fraction of CPDs in PVC) CPDs/PVC film at different excitation wavelength, respectively. (e) The PL spectra of LED based on different doping concentrations oABT-TSA-CPDs/PVC composites (395 nm LED chip; inset: Photo of the prepared LED). (f) The CIE coordinate of prepared LED.

with solution. Actually, PLQY was proportional to K_r/K_{nr}. The K_r/K_{nr} value of oABT-TSA-CPDs powder was 3.24 much larger than that of their solution (0.08), which also explained the higher PLQY in solid state.

To further verify the importance of the dissipation path of energy, PL spectrum and decay curves of oABT-TSA-CPDs powder under different temperatures were carried out (Figs. 3b and c, Fig. S6 in Supporting information). As the temperature decreased from 468 K to 78 K, the fluorescence became stronger, and the lifetime increased from 1.43 ns to 4.43 ns, which indicated that the non-radiative transition was inhibited. In conclusion, suppression of non-radiative transition played critical roles in high PLQY in solid state.

Non-radiative transition was related to the motion of PL center [27,28]. In CPDs, the surface state was free-moving in the solution, conducted to non-radiative transition. However, in solid state, the decreased distance among oABT-TSA-CPDs particles would be beneficial to restrict the movement of fluorescent chromophore and prevent non-radiative transition. Above all, the immobilization of surface state was the critical reason for the enhancement of solid-state fluorescence.

Furthermore, we used polyvinyl chloride (PVC) as matrix to restrict the movement of surface state in oABT-TSA-CPDs and explore the roles of fixation in their solid-state fluorescence enhancement. The PL spectra of 1% (the mass fraction of oABT-TSA-CPDs in PVC) oABT-TSA-CPDs/PVC (Fig. 4a) exhibited dual-peak emission, located at 407 nm and 470 nm, which represented carbon core state and surface state, respectively. Compared with the fluorescence spectra and the PL decay curve of the pure oABT-TSA-CPDs solution, the composite exhibited stronger surface state emission and longer lifetime (Tables S4 and S5 in Supporting information), demonstrating the fixation of PVC could inhibit the non-radiative transition of the surface state in oABT-TSA-CPDs, which proved the immobilization played a vital role in the enhanced fluorescence.

Besides, FTIR spectra (Fig. S7 in Supporting information) of oABT-TSA-CPDs and oABT-TSA-CPDs/PVC composite showed that the peak of O-H became broader and the peak of C=O functional group moved to low-frequency wavenumbers from dispersed state (in PVC) to aggregated state, which confirmed the formation of hydrogen bonds [30,31]. Based on our previous work, the hydrogen bond could act as cross-linking fixation of CPDs, inhibiting the non-radiative transition, thus enhancing the fluorescence. This phenomenon is called the crosslink enhanced emission (CEE) [27,28]. Therefore, the formation of hydrogen bonds in powder was also conductive to the enhanced fluorescence.

Additionally, the effect of concentration on fluorescence behavior was investigated. The PL intensity (Fig. S9 in Supporting information) of oABT-TSA-CPDs solution (DMF solution) increases first and then decreases as the increase of concentration. The molecule state peak appeared at high concentration (50 mg/mL and 100 mg/mL) but show weak emission. Therefore, in solution, the surface state is in free motion, and the oABT-TSA-CPDs shows weak fluorescence.

Interestingly, with the increase of the concentration of oABT-TSA-CPDs doping (3%, 5%, 10%), the fluorescence peak of the surface state was gradually apparent, while the peak of the carbon core state became weakened (Figs. 4b-d and Table S4). Besides, the PL decay curves (Fig. S8 and Table S5 in Supporting information) of these composites showed two PL centers, carbon core state (short lifetime) and surface state (long lifetime). With the increase of oABT-TSA-CPDs concentration, the proportion of carbon core state components gradually reduced (Tables S4 and S5). In addition, the oABT-TSA-CPDs powder only showed the surface state emission and exhibited monoexponential PL decay curve (Figs. 1c, 3a), suggesting that the fluorescence of carbon core state disappeared in powder [32].

By comparing the PL spectrum of oABT-TSA-CPDs solution (representing the emission of carbon core state) with the UV-vis absorption spectrum of oABT-TSA-CPDs powder (representing absorption of surface state), a significant overlap was observed (Fig. S10 in Supporting information), indicating surface state could resorb the emission of carbon core state, which explained the disappearance of carbon core state in solid state. In addition, the surface state showed 470 nm emission in dispersed state (solution and oABT-TSA-CPDs/PVC composites), but exhibiting 477 nm in powder, which was related to the interaction between CPDs particles in the aggregated state. It could be also proved by the broader and red shift of UV-vis spectra of oABT-TSA-CPDs powder comparing with that of solution (Fig. S10).

Above all, the schematic diagram of the mechanism about oABT-TSA-CPDs solid-state fluorescence enhancement was promoted in Fig. S11 (Supporting information). There were two PL centers in oABT-TSA-CPDs: carbon core state (407 nm) and surface state (470 nm in dispersed state and 477 nm in aggregated state), and the latter one dominated the solid-state fluorescence enhancement. The energy was mainly dissipated by non-radiative transition due to the free movement of the surface state, thus presenting weak emission in solution. But in solid state, the decreased distance between particles restricted the motion of surface state, and the formed hydrogen bonds could be also benefit for CEE [33], which both suppressed the non-radiative transition, and the emission of carbon core state was absorbed and reused, thus showing strong solid-state fluorescence.

Efficient solid-state luminescent CDs will broaden the application in the field of solid-state luminescent devices. oABT-TSA-CPDs/PVC was successfully utilized to fabricate photoluminescent LED. The electroluminescence (EL) spectra (Fig. 4e) showed that as the concentration of oABT-TSA-CPDs in composites increased, the EL intensity became higher. There were two peaks at 395 nm and 480 nm representing the UV-chip and oABT-TSA-CPDs powder, respectively. The photo of LED device showed bright blue-green light, which CIE coordinate (Fig. 4f) was at (0.17, 0.32). In view of these impressive performances and the advantages of simple synthetic method, low cost, oABT-TSA-CPDs has potential applications in solid-state lighting and display.

In summary, highly efficient solid state luminescent oABT-TSA-CPDs with PLQY up to 76% in powder without matrix were successfully synthesized by one step solvothermal method. By analyzing the structures of CPDs prepared under different conditions (reaction temperature and time), the PL centers of the oABT-TSA-CPDs were confirmed to be carbon core state (407 nm) and surface state (470 nm in dispersed state and 477 nm in powder), which was verified to be the potential fluorescence chromophore associated with carbonyl group. Additionally, the surface state dominated the fluorescent enhancement in solid state, which was different from other CDs like CQDs graphene quantum dots and some CPDs with high carbonization-degree. Based on the time-resolved PL decay curves and PL spectrum in different temperature, and the properties of oABT-TSA-CPDs/PVC composites, the fixation of surface state which inhibited the non-radiative transition was proved as the reason for the enhancement of solid-state fluorescence, additionally, the formation of hydrogen bonds during the aggregation process were also conductive to crosslinking and fixing. Finally, oABT-TSA-CPDs were successfully applied to the photoluminescence LED device. We believe that oABT-TSA-CPDs of high-performance fluorescent property could have superior performance in the fields of lighting and displays, biology, and photovoltaic devices.

Declaration of competing interest

The authors declare that they have no known competing financial interests or personal relationships that could have appeared to influence the work reported in this paper.

Acknowledgments

This work is supported financially by the National Science Foundation of China (Nos. 22035001, 21774041), and Jilin University Science and Technology Innovative Research Team (No. 2017TD-06).

Supplementary materials

Supplementary material associated with this article can be found, in the online version, at doi:10.1016/j.cclet.2022.107900.

References

[1] B. Wang, S. Lu, Matter 5 (2022) 110–149.
[2] J. Liu, S. Lu, Q. Tang, et al., Nanoscale 9 (2017) 7135–7142.
[3] G. Filippini, F. Amato, C. Rosso, et al., Chem 6 (2020) 3022–3037.
[4] F. Yuan, T. Yuan, L. Sui, et al., Nat. Commun. 9 (2018) 2249.
[5] F. Yuan, Y. Wang, G. Sharma, et al., Nat. Photonics 14 (2020) 171–176.
[6] K. Bramhaiah, R. Bhuyan, S. Mandal, et al., J. Phys. Chem. C 125 (2021) 4299–4309.
[7] E. Liu, D. Li, X. Zhou, et al., ACS Sustainable Chem. Eng. 7 (2019) 9301–9308.
[8] A. Xu, G. Wang, Y. Li, et al., Small 16 (2020) 2004621.
[9] C. Wang, T. Hu, Y. Chen, et al., ACS Appl. Mater. Interfaces 11 (2019) 22332–22338.
[10] Y. Wu, H. Zhang, A. Pan, et al., Adv. Sci. 6 (2019) 1801432.
[11] F. Yan, Y. Jiang, X. Sun, et al., Nano. Res. 13 (2020) 52–60.
[12] W. Liu, S. Xu, S. Guan, et al., Adv. Mater. 30 (2018) 1704376.
[13] Y. Ding, S. Cheng, Q. Chang, et al., ACS Sustainable Chem. Eng. 7 (2019) 14677–14684.
[14] J. Shao, S. Zhu, H. Liu, et al., Adv. Sci. 4 (2017) 1700395.
[15] Q. Chang, S. Yang, C. Xue, et al., Nanoscale 11 (2019) 7247–7255.
[16] J. Liu, R. Li, B. Yang, ACS Cent. Sci. 6 (2020) 2179–2195.
[17] Q. Zeng, T. Feng, S. Tao, S. Zhu, B. Yang, Light Sci. Appl. 10 (2021) 142.
[18] Z. Zhou, P. Tian, X. Liu, et al., Adv. Sci. 5 (2018) 1800369.
[19] H. Yang, Y. Liu, Z. Guo, et al., Nat. Commun. 10 (2019) 1789.
[20] Q. Wang, S. Zhang, B. Wang, et al., Nanoscale Horiz. 4 (2019) 1227–1231.
[21] T. Feng, Q. Zeng, S. Lu, et al., ACS Photonics 5 (2017) 502–510.
[22] B. Wang, Z. Wei, L. Sui, et al., Light Sci. Appl. 11 (2022) 172.
[23] X. Yang, L. Ai, J. Yu, et al., Sci. Bull. 67 (2022) 1450–1457.
[24] Y. Song, S. Zhu, S. Zhang, et al., J. Mater. Chem. C 3 (2015) 5976–5984.
[25] D. Chao, W. Lyu, Y. Liu, et al., J. Mater. Chem. C 6 (2018) 7527–7532.
[26] S. Tao, S. Lu, Y. Geng, et al., Angew. Chem. Int. Ed. 57 (2018) 2393–2398.
[27] S. Tao, S. Zhu, T. Feng, C. Zheng, B. Yang, Angew. Chem. Int. Ed. 59 (2020) 9826–9840.
[28] S. Zhu, Y. Song, J. Shao, X. Zhao, B. Yang, Angew. Chem. Int. Ed. 54 (2015) 14626–14637.
[29] Y. Zhang, X. Liu, Y. Fan, et al., Nanoscale 8 (2016) 15281–15287.
[30] C. Xia, S. Zhu, S. Zhang, et al., ACS Appl. Mater. Interfaces 12 (2020) 38593–38601.
[31] T. Meng, T. Yuan, X. Li, et al., Chem. Commun. 55 (2019) 6531–6534.
[32] D. Zhou, P. Jing, Y. Wang, et al., Nanoscale Horiz. 4 (2019) 388–395.
[33] S. Tao, C. Zhou, C. Kang, et al., Light Sci. Appl. 11 (2022) 56.